Arabian Journal for Science and Engineering (2022) 47:7023–7033
https://doi.org/10.1007/s13369-021-06300-4

RESEARCH ARTICLE-CHEMISTRY

Effectiveness of Ru/Mg/Ce Supported on Alumina Catalyst for Direct Conversion of Syngas to Methane: Tailoring Activity and Physicochemical Studies

Susilawati Toemen[1] · Siti Fadziana Sulaiman[1] · Salmiah Jamal Mat Rosid[2] · Wan Azelee Wan Abu Bakar[1] · Wan Nur Aini Wan Mokhtar[3] · Renugambaal Nadarajan[1] · Khalida Muda[4] · Sarina Mat Rosid[5]

Received: 5 March 2021 / Accepted: 12 October 2021 / Published online: 9 November 2021

Abstract

The century of urbanisation and industrialisation had a great impact on the environment due to the rapid growth of the flue gas sectors. Thus, green technology is enforced to convert carbon dioxide (CO_2) gas into methane (CH_4) gas as an alternative fuel in electricity generation, particularly coal and natural gas sources. Cerium (Ce) was recognised as one of the most basic and unique redox characteristics utilised in the promising methanation reaction among catalysts used. The trimetallic catalyst used in this work was prepared with Ce as the based catalyst and ruthenium/magnesium (Ru/Mg) as the impregnated metal. Response surface methodology projected the CO_2 conversion to be less than 0.3% of the experimental value of 78.82% using the indicated parameters of 593 °C calcination temperature and 61 wt.% ratios. Ru/Mg/Ce/Al_2O_3 catalyst with 60 wt.% of Ce loading calcined at 600 °C produced 58.08% of CH_4. The characterisation results revealed that CeO_2, $Mg(Al_2O_4)$, and RuO_2 species were the active species for CO_2 methanation selectivity, as observed in XRD and XPS analyses. The mesoporous structure and particle agglomeration resulted in a surface area of 147 m^2/g.

Keywords Methanation · Power plant · Carbon dioxide · Catalyst · Cerium based

1 Introduction

Numerous power plant stations have been built worldwide due to urbanisation and industrialisation, primarily in coal, gas, and oil for combustion process. However, flue gases released into the atmosphere by combustion are hazardous. Carbon dioxide (CO_2) is the most harmful greenhouse gas compound that causes climate change. In developing and industrial countries, the growing fuel consumption is inevitable [1–3]. Therefore, these countries are creditworthy to the more significant emitter along with their economic growth. At present, the topic of methanation has been extensively explored, while numerous technologies for CO_2 recovery have been introduced. Chemical absorption is a technique for separating CO_2 gas from flue gases by using several amines as absorbent. Flue gases generally enter the absorber, while the absorbent chemically reacts with CO_2 in the flue gases. Besides, CO_2 can be reduced using polymer membrane, a relatively new technology discovered to remove CO_2. Similar to chemical absorption, CO_2 gas is separated from flue gases via thin layer, in which selective transport occurs and is driven by pressure difference across

✉ Susilawati Toemen
susilawatitoemen@utm.my

✉ Salmiah Jamal Mat Rosid
salmiahjamal@unisza.edu.my

1 Department of Chemistry, Faculty of Science, Universiti Teknologi Malaysia, UTM, 81310 Johor Bahru, Johor, Malaysia

2 Unisza Science and Medicine Foundation Centre, Universiti Sultan Zainal Abidin, Kampus Gong Badak, 21300 Kuala Nerus, Terengganu, Malaysia

3 Department of Chemical Sciences, Faculty of Science and Technology, Universiti Kebangsaan Malaysia, 43600 Bangi, Selangor, Malaysia

4 Department of Environmental Engineering, Faculty of Civil Engineering, Universiti Teknologi Malaysia, UTM, 81310 Johor Bahru, Johor, Malaysia

5 Advanced Membrane Technology Research Centre (AMTEC), Universiti Teknologi Malaysia, UTM, 81310 Johor Bahru, Johor, Malaysia

the membrane [4, 5]. However, both technologies incur high operating cost, whereas the materials and installations must be compatible with the operation parameters, such as pressure and temperature.

Among the available technologies, methanation reaction via hydrogenation is the most practical method for CO_2 reduction. The efficacy of this approach in converting CO_2 to entirely methane gas at a low cost has been vastly reported. The said approach can treat a huge amount of CO_2 in less time and at a lower reaction temperature. The methane produced from the reaction is clean fuel that may be deployed to power turbines for electricity generation. Most methane is derived from fossil fuels, but this contributes to global environmental problems. As a result, much attention is given to conversion of carbon oxide-rich gases to methane or methanation [6]. The CO_2 methanation reaction is thermodynamically favourable at low temperatures, but kinetic restrictions necessitate a catalyst to convert fully oxidised carbon to methane. Considerable efforts have been devoted in researching various aspects of CO_2 methanation catalysts.

Transition metals catalysts have been thoroughly studied as active catalysts for CO_2 hydrogenation [7], along with their effects on CO_2 activation and reduction steps. Iron, cobalt, nickel, and copper are among those with high catalytic activity for CO_2 methanation. Ceria (Ce) has also been investigated as single support for efficient Ni catalysts in CO_2 methanation [8, 9]. However, Ce as a catalyst still receives minimal reviews in methanation reaction; even Ce provides unique redox properties, as well as high oxygen storage capacity and mobility [10]. Previous studies demonstrated that Ce was rarely used solely [11]. However, combining other metal oxides by doping or modifying the preparation procedure could result in Ce catalysts with a high degree of textural stability [12]. Furthermore, Mg was once added to a Ni-based catalyst for methanation reaction and appeared to be one of the elements capable of increasing catalyst activity [13]. Meanwhile, Ru can assist in improving catalytic conversion while also providing stability to the catalyst [14].

Recently, researchers have successfully studied the potential of cerium as catalyst in providing higher CO_2 conversion (97.73%) and 91.31% CH_4 formation using Ru/Mn/Ce(5:30:65)/Al_2O_3 catalyst in flue gases [11], as well as 100% CO_2 conversion and 80% CH_4 formation using Ru/Mn/Ce (5:35:60)/Al_2O_3 for CO_2 methanation in simulated natural gas [15]. The trimetallic oxide catalysts are favourable due to the lower performance of bimetallic oxide catalyst that requires high operating reaction temperature, thus limiting the application in large-scale industrial segments. Rosid et al. [6] found that the trimetallic oxide catalyst Ru/Mn/Nd (5:20:75)/Al_2O_3 revealed higher CO_2 conversion at 100% with 400 °C reaction temperature. This was ascribed to the addition of ruthenium (Ru) as co-dopant that improved the catalytic activity on CO_2 conversion as the presence of Ru favoured the reduction process and dispersion on the surface of the catalyst. Meanwhile, Zamani et al. used trimetallic oxide catalyst and reported higher CO_2 conversion by varying a series of Ru content promoted on Cu/Mn and supported onto Al_2O_3 [16].

Due to the superior performance of trimetallic oxide catalyst, new mixed oxide catalysts using Ce, Mg, and Ru were synthesised using the wetness impregnation method. The combination of these metal oxides is expected to increase CO_2 conversion and to enable higher methane conversion. To better understand the role of Ru/Mg/Ce catalyst in methanation reaction, the catalyst was designed and optimised using the statistical design of response surface methodology (RSM) by deploying different dopants, co-dopants, and calcination temperatures. The parameters of calcination temperature and Ce-based loading were selected because these two factors contribute the most significant impact on catalytic performance [15]. Meanwhile, Central Composite Design (CCD) was selected because this design can fit a full quadratic model and has more design points to determine the optimal setting for each factor [17].

2 Materials and Methods

2.1 Preparation of Catalysts

The catalysts were synthesised using the wet impregnation method with nitrate and chloride salts from Sigma-Aldrich as metal precursor, as described in our previous work [6]. First, 5 g of $Ce(NO_3)_3{\cdot}6H_2O$ was dissolved in 10 mL of distilled water in a beaker. Next, the solution was mixed with the promoter salts solutions of $Mg(NO_3)_2{\cdot}6H_2O$ (8.51 g) and $RuCl_3{\cdot}3H_2O$ (0.55 g) and then stirred continuously for 30 min at room temperature with a magnetic bar until the solution was homogenised. After that, 10 g of alumina beads with an average diameter of 4–5 mm was immersed in a metal salt solution prepared for a certain time before being aged in an oven at 80–90 °C for 24 h. Then, the catalysts were calcined at 500 °C for 5 h with a ramp rate of 10 °C/min. Finally, the samples were labelled as Ru/Mg/Ce (10:30:60)/Al_2O_3, indicating the presence of 60 wt.% of Ce, 30 wt.% of Mg, and 10 wt.% of Ru. Similar procedures were applied for other desired ratios of Ru/Mg/Ce (10:35:55)/Al_2O_3 and Ru/Mg/Ce (10:25:65)/Al_2O_3 catalysts with Ce content of 55 wt.% and 65 wt.%, respectively, as well as calcination temperatures of 600 °C and 700 °C, respectively.

2.2 Catalytic Activity Measurement

The performance of the prepared catalysts was evaluated under atmospheric pressure in a fixed bed micro-reactor coupled with Fourier transform infrared (FTIR) spectroscopy.

The 10 g of supported catalyst was placed in the centre of a Pyrex glass tube with a diameter of 10 mm and a length of 520 mm. The experiment was continued by simulating power station flue gases that consisted of CO_2, H_2, and compressed air with the ratio of 10:40:50%vol, as well as reaction temperature ranging from room temperature to 300 °C. The gas flow was passed through the catalyst at varying temperature reactions, with 1 h of retained time for each reaction temperature. The total flow rate was set to 100 mL/min, with the gas hourly space velocity (GHSV) remained constant at 510 h^{-1}. The product composition was collected in FTIR gas cell attached with KBr windows and scanned with FTIR Thermo Scientific Nicolet iS10, while CH_4 formation was analysed using GC-FID (Hewlett Packard 6890 Series GC System).

2.3 Catalysts Characterisation

The N_2 adsorption/desorption isotherm (NA) analysis of the catalyst was executed using a Micromeritics ASAP 2010 volumetric adsorption analyser at − 196 °C. Before the measurement, the calcined catalysts were degassed at 120 °C overnight. The catalyst structure was determined via X-ray diffraction (XRD) using Cu Kα radiation ($\lambda = 1.54060$ Å). Data were collected over the range of 2θ from 20 to 80°. X-ray photoelectron spectroscopy (XPS) analysis was performed using Kratos AXIS Ultra DLD with 15.0 kV energy. The samples were tested at the electron take-off angle normal to the surface working at 20 eV. The surface morphology of the catalyst was obtained by using field emission scanning electron microscopy (FESEM) Zeiss Supra 35VP FESEM with 15.0 kV energy coupled with a EDX analyser. Energy-dispersive X-ray (EDX) was also used to determine the elemental composition on the submicron scale.

2.4 Response Surface Methodology (RSM)

The experimental results were validated by comparing them to the RSM-predicted outcomes of the optimisation parameter. The Design-Expert version 7.1.6 software was used to generate and evaluate the statistical experimental design for RSM. The response surface was described using an empirical model based on a second-order polynomial Eq. (1):

$$Y = \beta 0 + \Sigma\, \beta i Xi + \Sigma\, \beta ii Xi^2 + \Sigma\, \beta ij Xi Xj \quad (1)$$

where Y is the response and $\beta 0$, βi, βii, and βij are coefficients of the intercept, linear, square, and interaction effects.

Presumably, CO_2 conversion would be significantly affected by two independent factors: calcination temperature (X_1) and Ce-based loading (X_2) [11]. The CCD procedure was conducted to optimise CO_2 conversion (%) for two factors using $22 = 4$ factorial points with 13 experiments. The detailed reaction conditions are presented in Table 1.

3 Result and Discussion

3.1 Optimisation of Ru/Mg/Ce/Al_2O_3 Catalyst

Various catalyst compositions were investigated to determine the most promising catalyst that can improve CO_2 methanation performance. The Ce loading was initially adjusted from 70 wt.% to 55 wt.%, and the CO_2 conversion trend is illustrated in Fig. 1. Based on Fig. 1a, Ru/Mg/Ce (10:20:70)/Al_2O_3 catalyst calcined at 400 °C converted approximately 50.74% of CO_2, whereas 65 wt.% Ce catalyst converted around 57.09% at a maximum reaction temperature of 300 °C. As the Ce loading was further reduced at a similar reaction temperature, the CO_2 conversion increased to 60.61%. However, after that point, the percentage of CO_2 conversion fell to 48.59%. This was attributed to the agglomeration on the catalyst surface, as depicted by Toemen et al. [11]. As a result, the catalyst performance trend was 55 wt.% < 70 wt.% < 65 wt.% < 60 wt.%. The Ru/Mg/Ce catalyst calcined at 400 °C was further studied at a calcination temperature of 600 °C. Figure 1b demonstrates that Ce loading at 60 wt.% kept performing higher CO_2 conversion with a reading of 79.04% at maximum reaction temperature of 300 °C. Meanwhile, Ce loading of 70 wt.%, 65 wt%, and 55 wt.% resulted in CO_2 conversion of 65.74%, 69.53%, and 67.11%, respectively. Since the Ru/Mg/Ce (10:30:60)/Al_2O_3 catalyst calcined at 600 °C performed better than other catalysts, it was then extended to several calcination temperatures. Figure 2 portrays the trend of CO_2 conversion as a function of calcination temperatures over this catalyst.

The catalytic activity of the catalysts was noticeably affected by calcination temperatures, as shown in Fig. 2. Overall, the conversion of CO_2 to methane was aided by increasing the calcination temperature. According to Perego and Villa [18], some processes, including sintering-induced changes in structure and texture, active phase formation, loss of chemically linked CO_2, and H_2O stability of chemical properties, may occur during the calcination process. These are consistent with our findings, which increased the performance of the catalysts with calcination temperature increment from 300 to 600 °C. At the reaction temperature of 300 °C, the Ru/Mg/Ce (10:30:60)/Al_2O_3 catalyst calcined at 600 °C showed immense increase in CO_2 conversion that contributed up to 79.04% of CO_2. Nonetheless, at higher calcination temperatures (> 600 °C), the conversion percentage dropped due to particle enlargement, as evidenced in XRD and N_2 adsorption analysis.

Table 2 shows the methane formation over a potential catalyst of Ru/Mg/Ce(10:30:60)/Al_2O_3 calcined at 600 °C. Two

Table 1 The coded and uncoded level of the independent variables

Run	X_1: Calcination T (°C)	X_2: Loading of Ce (wt.%)	CO_2 Conversion (%)	
			Actual	Predicted
1	− 1 (500)	− 1 (55)	45.76	44.53
2	− 1.414 (458.58)	0 (60)	43.87	45.11
3	− 1 (500)	1 (65)	63.30	62.25
4	0 (600)	0 (60)	79.02	78.01
5	1 (700)	− 1 (55)	50.48	49.76
6	1 (700)	1 (65)	52.35	51.80
7	0 (600)	− 1.414 (52.93)	52.90	53.91
8	0 (600)	0 (60)	79.04	78.01
9	0 (600)	1.414 (67.07)	67.13	67.89
10	0 (600)	0 (60)	78.83	78.01
11	0 (600)	0 (60)	74.78	78.01
12	1.414 (741.42)	0 (60)	40.89	41.42
13	0 (600)	0 (60)	78.40	78.01

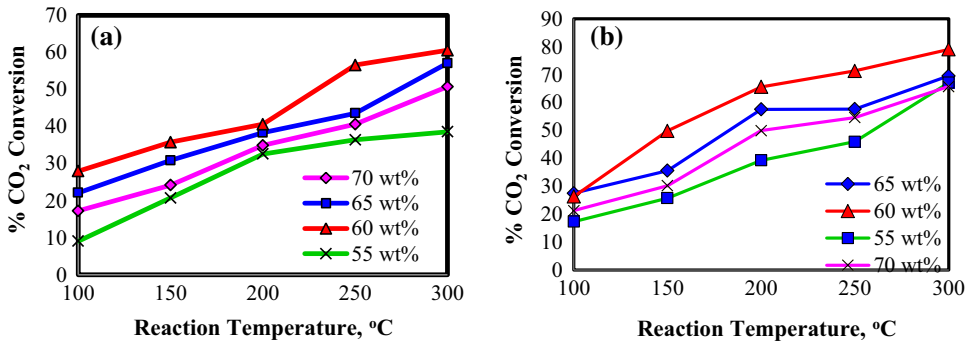

Fig. 1 Catalytic performance of CO_2 conversion over $Ru/Mg/Ce/Al_2O_3$ catalysts at various ratio of Ce based, calcined at **a** 400 °C and **b** 600 °C for 5 h

Table 2 Products obtained from CO_2 methanation reaction over $Ru/Mg/Ce(10:30:60)/Al_2O_3$ catalyst via gas chromatography

Catalyst	Reaction temperature (°C)	Products (%)		Unreacted CO_2 (%)
		CH_4	By-product $CO + H_2O$	
$Ru/Mg/Ce(10:30:60)/Al_2O_3$	100	0.00	19.70	80.30
	200	37.86	27.76	34.38
	300	58.08	20.96	20.96

main products, methane and water, were obtained during the reaction process. The CO_2 was obviously transformed into CH_4 and a by-product, while the fraction of unreacted CO_2 was reduced. Meanwhile, the CH_4 product increased in tandem with the reaction temperature. At 100 °C, the methane product was not yet produced. Still, by-products, such as CO and H_2O, were produced, which is in good agreement with the findings reported by Yaccato et al. [19], in which their reaction yielded CO at lower temperatures, while CH_4 was formed at higher temperature. At the highest examined temperature of 300 °C, the maximum product of CH_4 formed was 58.08%, which was ascribed to the rapid hydrogenation of intermediate CO species into CH_4 products.

3.2 Optimisation of $Ru/Mg/Ce/Al_2O_3$ Catalyst by RSM

The RSM was applied over $Ru/Mg/Ce/Al_2O_3$ catalyst to validate the optimisation value derived from the experimental data. In order to determine the optimum reaction parameters toward CO_2 conversion (Y), two factors were taken into consideration—catalyst calcination temperature (X_1) and loading of Ce (X_2). The following quadratic equation (Eq. 2) depicts the relationship between these two independent variables and the dependent response is as follows:

$$Y = 78.01 - 1.31 * X_1 + 4.94 * X_2 - 3.92 * X_1 * X_2 - 17.37 * X_1^2 - 8.56 * X_2^2 \quad (2)$$

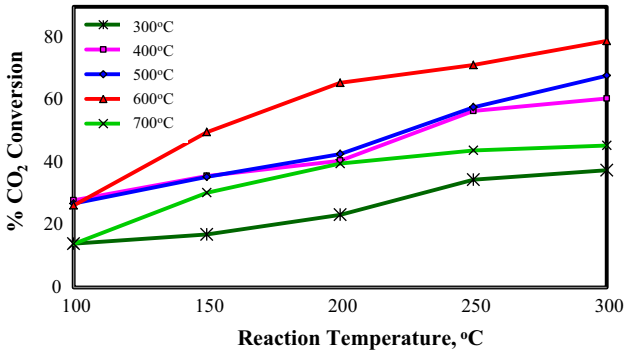

Fig. 2 Effect of calcination temperatures over Ru/Mg/Ce (10:30:60)/Al_2O_3 catalyst

The actual and predicted values of CO_2 conversion obtained from the design model are presented in Table 1. Figure 3a demonstrates the plotted graphical regression for the comparison of these values. The point distributions were relatively close to the linear line, implying good agreement between the predicted and actual values in the specific range of experiments. Meanwhile, Table 3 shows the analysis of variance (ANOVA) that was used to validate the model and the results obtained from the model. According to Kousha et al., the significance of each coefficient was determined by F value and p value from the designated model [20, 21]. These values were used to decipher the pattern and the interactions of the test variables. The F value from the design model was 183.56, with a low p value of <0.0001, indicating that the model was significant with only 0.01% chance that the model value occurred due to noise. The p value should be less than 0.05 to indicate the significance of the model terms. Thus, the design model for CO_2 conversion study was indeed significant.

The design displayed lack of fit (modelling error) value of 0.69, implying the lack of fit was not statistically significant in comparison with pure error (experimental error). The acquired R^2 value indicated that the regression model explained 99.24% of the experimental results, with ~0.76% of the total variance remaining unaccounted by this model and that the model fitted the experimental data. Meanwhile, the adjusted R^2 value was 0.9870 and the predicted R^2 value was 0.9739. The R^2 value agreed with both the adjusted and predicted R^2 values. The results demonstrated a strong correlation between observed and predicted values.

Adequate precision (known as signal-to-noise ratio) was 31.699 [22]. A ratio greater than 4 is necessary to obtain an adequate signal. Thus, a ratio of 31.699 signified high reliability of the experimental data, whereby the model could be used to navigate the design space. High reliability toward the experimental data was determined by lower values of coefficient of variation, CV (2.74%), and standard deviation, SD (1.70). The low predicted residual sum of squares (PRESS) at 69.71 showed that the model had good fit with each point in the model [20]. Overall, significant F value, insignificant p value, high R^2 value, adequate high precision, and low PRESS indicated that the model had high adequacy and validity in predicting CO_2 conversion.

The three-dimensional (3D) response surface and two-dimensional (2D) contour plot generated by the software illustrated the interaction between the two variables with the response toward CO_2 conversion. The response surface (see Fig. 3b) displayed an elliptical model graph, indicating that the interaction between the variables was valid for CO_2 conversion. Notably, CO_2 conversion increased as the calcination temperature of the catalyst increased, particularly when it began at 500 °C as the calcination temperature. However, as the calcination temperature reached beyond 650 °C, the CO_2 conversion slightly decreased. The highest CO_2 conversion was noted at 600 °C of catalyst calcination temperature. Therefore, the optimal calcination temperature for CO_2 conversion was between 550 and 650 °C. The plot obtained agreed with the experimental data, whereby CO_2 conversion was the highest when the catalyst was calcined at 600 °C. It could be explained that the high-temperature catalyst agglomerated and formed larger particles, thus reducing the surface area of the catalyst.

Based on the second factor—the catalyst ratio—the contour plot showed higher CO_2 conversion as the catalyst ratio rose. However, at above 58 wt.% of catalyst ratio, a circular contour was observed, indicating that the interaction with the catalyst ratio resulted in nearly similar CO_2 conversion. According to the results, the catalyst with 60 wt.% ratio yielded the highest CO_2 conversion. Reasonably, the contour plot obtained is in agreement with the experimental data.

The ideal circumstances were determined by defining goals for each parameter, such as catalyst calcination temperature of 550–650 °C and ratio of catalyst of 55–65 wt.%. With the suggested parameters of calcination temperature at 593 °C and a ratio at 61 wt.%, the CO_2 conversion was anticipated to be less than 0.3% of the experimental value of 78.82%, as shown in Table 4. An additional experiment was carried out under specified ideal conditions, and the results revealed that CO_2 conversion was 78%, nearly identical to the proposed solution. Therefore, the regression model is in line with the experimental findings, thus validating the outcomes of response surface optimisation.

3.3 Characterisation

3.3.1 Nitrogen Adsorption Analysis

Table 5 presents the textural properties of commercial γ-Al_2O_3 and Ru/Mg/Ce/Al_2O_3 catalysts prepared with different ratios and calcination temperatures. Based on the table, commercial γ-Al_2O_3 exhibited the highest surface area of

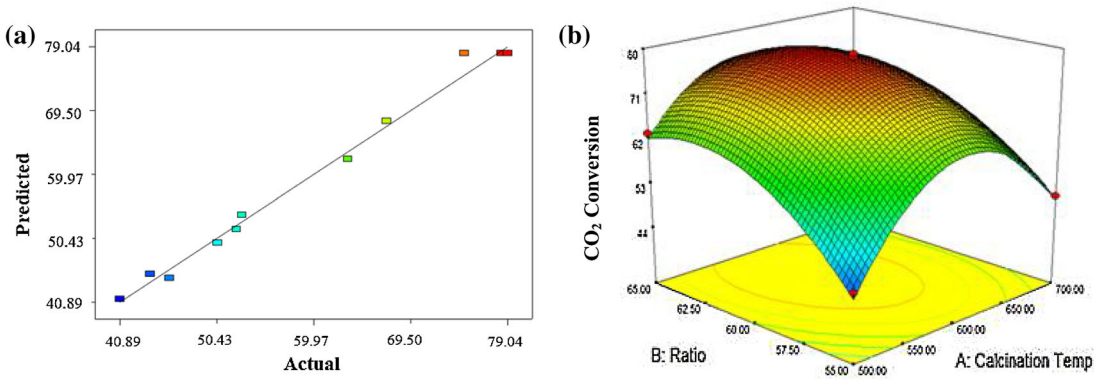

Fig. 3 **a** Relationship between actual and predicted values of the quadratic model, **b** 3-D response surface contour plot for CO_2 conversion

Table 3 ANOVA results of the response surface quadratic model for CO_2 conversion

Source	Freedom degree	Sum of squares	Mean square	*F* value	*p* value
Model	5	2650.04	530.01	183.56	<0.0001[a]
X_1	1	13.64	13.64	4.72	0.0663
X_2	1	195.37	195.37	67.66	<0.0001
X_1X_2	1	61.39	61.39	21.26	0.0025
X_1^2	1	2099.69	2099.69	727.21	<0.001
X_2^2	1	509.22	509.22	176.37	<0.001
Residual	7	20.21	2.89		
Lack of fit	3	6.87	2.29	0.69	0.6054[b]
Pure error	4	13.34	3.33		
Total	12	2670.25			

Std deviation = 1.70, mean = 62.06, CV (%) = 2.74, PRESS = 69.71, R^2 = 0.9998, R^2 (adj) = 0.9996, R^2 (pred) = 0.9992, adequate precision = 31.70, [a] significant; [b] not significant

Table 4 Constraints of each factor for the maximum CO_2 conversion

	Name	Goal	Lower limit	Upper limit	Optimal condition
X_1	Calcination temperature, °C	In range	550	650	593
X_2	Ratio of catalyst, wt.%	In range	55	65	61
Y	CO_2 conversion, %	Maximise	90	100	78.82

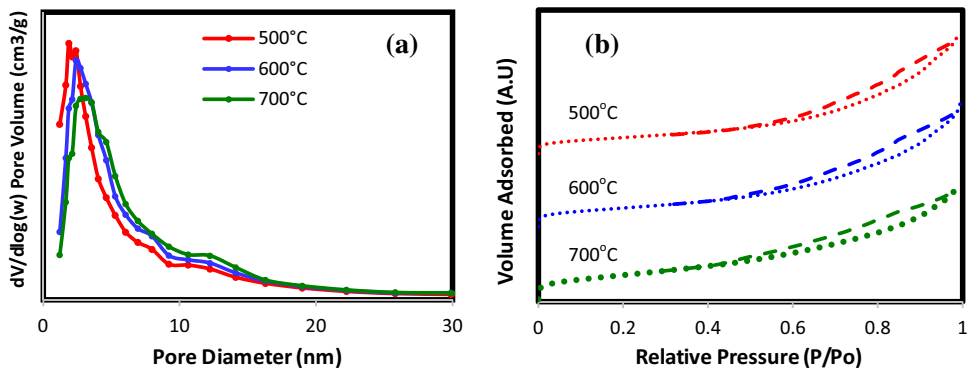

Fig. 4 **a** Pore size distributions of and **b** N_2 adsorption/desorption isotherms over Ru/Mg/Ce(10:30:60)/Al_2O_3 catalyst calcined at 500 °C, 600 °C and 700 °C for 5 h

249 m^2/g with an average pore diameter of 6.5 nm. However, a reduction in surface area was observed when the Ru/Mg/Ce catalyst was coated on the catalyst surface, attributable to the partially collapsed pore structure after its contact with the catalyst. When the calcination temperature of Ru/Mg/Ce (10:30:60)/Al_2O_3 catalyst was increased, the BET surface area decreased from 189 to 131 m^2/g. This was due to the tendency of the particles to agglomerate at higher calcination

Table 5 Physical properties of Ru/Mg/Ce/Al_2O_3 catalyst at various ratios and calcination temperatures

Catalysts	Calc. Temp (°C)	BET surface area (m^2/g)	Average pore diameter (nm)	Average pore volume (nm)
Ru/Mg/Ce(10:35:55)/Al_2O_3	600	155	9.84	0.43
Ru/Mg/Ce(10:30:60)/Al_2O_3	500	189	7.91	0.42
Ru/Mg/Ce(10:30:60)/Al_2O_3	600	147	10.43	0.44
Ru/Mg/Ce(10:30:60)/Al_2O_3	700	131	11.81	0.43
Ru/Mg/Ce(10:25:65)/Al_2O_3	600	151	10.07	0.43
γ-Al_2O_3 (commercial)	–	249	6.5	0.40

temperature and the formation of larger particles [23, 24]. As the calcination temperature increased to 600 °C, the pore diameter of 500 °C-calcined catalyst shifted slightly to the right (see Fig. 4a). This shift indicated that the pore diameter of the catalyst expanded with the increment of calcination temperature. By rising the calcination temperature to 700 °C, the BET surface area was further decreased to 131 m^2/g. The lower BET surface area of the catalyst sample represented larger pore size in mesopores [25]. Therefore, the pore size obtained was greater with higher calcination temperature.

Additionally, the pore volume of all the catalysts ranged at 0.42–0.44 nm. There was no significant change in BET surface area, pore diameter, and pore volume when the catalyst composition was changed. The BET surface area of the catalyst containing 55 wt.% Ce was 155 m^2/g, while the surface area slightly decreased with a reading of 151 m^2/g over 65 wt.%. As shown by the N_2 adsorption/desorption isotherms of Ru/Mg/Ce/Al_2O_3 catalyst (see Fig. 4b), all the prepared catalysts exhibited Type H3 hysteresis loop, thus confirming Type IV isotherms with a typically mesoporous structure and capillary condensation with non-uniform slit shape pore. The Ru/Mg/Ce (10:30:60)/Al_2O_3 catalyst possessed a substantial capacity of mesoporous structure regardless of the calcination temperature. As the calcination temperature increased, the hysteresis loop obtained was slightly narrower, thus explaining that the degree of mesoporosity of the catalyst was higher at lower calcination temperature. Therefore, it could provide more inner surface area and active sites to the catalyst.

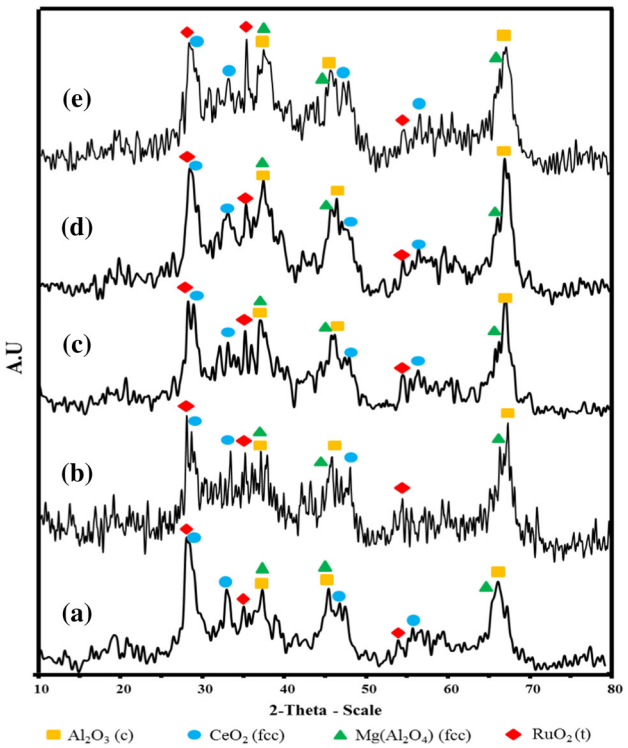

Fig. 5 XRD diffractograms for **a** Ru/Mg/Ce (10:35:55)/Al_2O_3 calcined at 600 °C, Ru/Mg/Ce (10:30:60)/Al_2O_3 catalyst calcined at **b** 500 °C, **c** 600 °C and **d** 700 °C and **e** Ru/Mg/Ce (10:25:65)/Al_2O_3 calcined at 600 °C for 5 h

3.3.2 X-ray Diffraction (XRD) Analysis

Figure 5 shows the XRD patterns of Ru/Mg/Ce/Al_2O_3 catalyst with varying ratios and calcination temperatures. Overall, all the catalysts were classified as polycrystalline phases, with the emergence of species Al_2O_3, CeO_2, $Mg(Al_2O_4)$, and RuO_2. The XRD patterns seemed identical, albeit different calcination temperatures and Ce-based loadings, indicating that the metal species were well dispersed across alumina surface. However, $Mg(Al_2O_4)$ species formed at lower calcination temperature as a result of solid-state reaction between MgO and alumina support during the heating process resulted in aluminate species.

Next, Al_2O_3 over Ru/Mg/Ce(10:30:60)/Al_2O_3 catalyst was present in cubic phase at 2θ of 67.263 (522), 37.044 (311), and 45.817° (400) at calcination temperature of 500 °C (see Fig. 5b). The 2θ of tetragonal RuO_2 was noted at 28.028 (110), 35.094 (101), and 54.413° (211). A difference was observed in Fig. 5b when compared to Fig. 5c and d. In Fig. 5b, the one peak that should represent the face-centred cubic CeO_2 at $2\theta = 56°$ was absent. This was ascribed to the poor crystallinity of the catalyst, which recorded high noise-to-signal ratio. From these findings, the CeO_2 species were only found at $2\theta = 28.580°$ (I_{100}), 47.288° (I_{52}), and 33.366° (I_{30}).

Table 6 EDX analysis of $Ru/Mg/Ce/Al_2O_3$ at different ratios and calcination temperatures

Catalysts	Calc. Temp (°C)	Weight ratio (%)				
		Al	O	Ce	Mg	Ru
$Ru/Mg/Ce(10:35:55)/Al_2O_3$	600	26.23	40.46	18.71	4.75	9.85
$Ru/Mg/Ce(10:30:60)/Al_2O_3$	500	27.01	33.95	23.64	3.93	11.47
$Ru/Mg/Ce(10:30:60)/Al_2O_3$	600	27.29	30.58	25.11	4.44	12.58

The $Mg(Al_2O_4)$ species was noted at $2\theta = 37.044°$ (I100), 66.288° (I57), and 45.187° (I49). In addition, a peak denoting the $Mg(Al_2O_4)$ species at $2\theta = 45°$ overlapped with the Al_2O_3 peak, resulting in the formation of a broad peak. During the heating process, a solid-state reaction occurred between MgO and alumina support to form aluminate species at low calcination temperatures below 800 °C (R). As the catalyst was calcined at 600 °C (see Fig. 5c), the existing species were the same as those found in the 500 °C catalyst. However, one peak of CeO_2 species that cannot be detected at 500 °C calcination temperature can be easily distinguished from the catalyst calcined at 600 °C ($2\theta = 56°$). The increase in calcination temperature had promoted the particle sizes to grow, thus increasing the intensity of the catalyst [26].

A similar pattern was attained for the catalyst calcined at 700 °C (see Fig. 5d). The overlapping of two individual peaks of CeO_2 and RuO_2 species obtained previously at 600 °C of calcination temperature resulted in high and broad peak at 2θ around 28. Meanwhile, the other CeO_2, RuO_2, and $Mg(Al_2O_4)$ species were positioned at their particular 2θ. These species, as expected, were in stable phases and were firmly positioned at almost the same location, even though the Ce loading of the catalyst differed. This occurred due to the presence of the same metal Ce on the alumina.

3.3.3 X-ray Photoelectron Spectroscopy (XPS) Analysis

Figure 6 shows the wide scan spectra for each element in $Ru/Mg/Ce/Al_2O_3$ catalyst samples: Al 2*p*, O 1 *s*, Ce 3d, and Mg 2*p*. The obtained spectra were nearly identical and remained unchanged, indicating that the calcination temperature and the composition factors did not affect the oxidation state of the species present. The existence of the oxidation state of the elements was confirmed based on their respective binding energies (Eb). However, due to an overlapping C 1 s peak at 284.50 eV, the Ru 3d peak could not be observed in this study.

From the spectra of Al 2*p*, the $Ru/Mg/Ce$ $(10:30:60)/Al_2O_3$ catalyst calcined at 500 °C (Al 2*p* (a)) displayed the existence of Al in different environments when compared to $Ru/Mg/Ce$ $(10:30:60)/Al_2O_3$ and $Ru/Mg/Ce(10:35:55)/Al_2O_3$ catalysts calcined at 600 °C. Three deconvolution peaks were observed at 73–76 eV. The contributions at E_b of 73.42 eV and 74.65 eV were due to Al^{3+} in Al_2O_3 and $Mg(Al_2O_4)$, respectively. Meanwhile, the peak at 76.28 eV was due to the formation of Al^{3+} in $Al(OH)_3$. When Al atom was on the outermost surface, alumina interacted with the atmosphere and absorbed water [27]. However, from Al 2*p* (b) and (c), Al was represented in two deconvolution peaks at a binding energy of 73–74 eV, indicating Al^{3+} in Al_2O_3 and $Mg(Al_2O_4)$. The peak due to $Al(OH)_3$ could not be detected, probably due to calcination at 600 °C. Due to the higher concentration of Al^{3+} species in Al_2O_3, the mass concentration for the peaks attributed to Al^{3+} in Al_2O_3 was higher (average: 10–25%) than the peak attributable to Al^{3+} in $Mg(Al_2O_4)$ (average: 4%).

Multiple peaks were noted for O 1 *s* species due to the overlapping of distinct chemical oxygen species surrounding the metal oxide of the catalyst. The deconvolution peaks at binding energy of 530–532 eV were identified as oxygen from oxides in the form of O^{2-} ions [27]. This was attributed to metal oxides of CeO_2, MgO, RuO_2, and Al_2O_3 species. Specifically, the literature depicts that the binding energy over three peaks of O 1 *s* as lattice oxygen (O_{lat}) (529.4–530.8 eV), surface-adsorbed oxygen such as O_2^{2-} or O^- (O_{ads}) (531.2 − 531.8 eV), and surface-adsorbed molecular water (O_{surf}) (above 533.0 eV) [28–32].

Furthermore, Ce^{4+} (CeO_2) was detected in the catalyst based on the binding energy determined from Ce 3*d* spectra. According to Truffault et al., the Ce 3*d* spectra region contained three pairs of doublets as (*x*, *y*), (*x*', *y*'), and (*x*", *y*") with x and y from $3d_{3/2}$ and $3d_{5/2}$ [29]. The $3d_{3/2}$ peaks for (a) can be found at binding energy of 900.87 eV, 907.47 eV, and 915.48 eV, while (b) can be found at $E_b = 900.94$ eV, 907.51 eV, and 915.41 eV, whereas (c) can be observed at $E_b = 902.72$ eV, 907. 74 eV, and 915.63 eV. The peaks represented cerium in its oxidised form, which belonged to the Ce^{4+} oxidation state from CeO_2 with respect to the final states of Ce $3d^9 4f^0$ O $2p^6$, Ce $3d^9 4f^1$ O $2p^5$, and Ce $3d^9 4f^2$ O $2p^4$ [28, 33]. Furthermore, the Ce peak near 916 eV indicated the presence of Ce^{4+} species [34]. For Ce^{4+} species, the mass concentration was around 15–20%.

The existence of Mg species was detected from the XPS technique. The Mg 2*p* spectrum could be deconvoluted into two pairs of components. The broad peak found at the binding energy of 49 eV was ascribed to $Mg(Al_2O_4)$ species, based on XPS NIST database. Meanwhile, the binding energy of MgO species was found at 50 eV [35]. Except for MgO species,

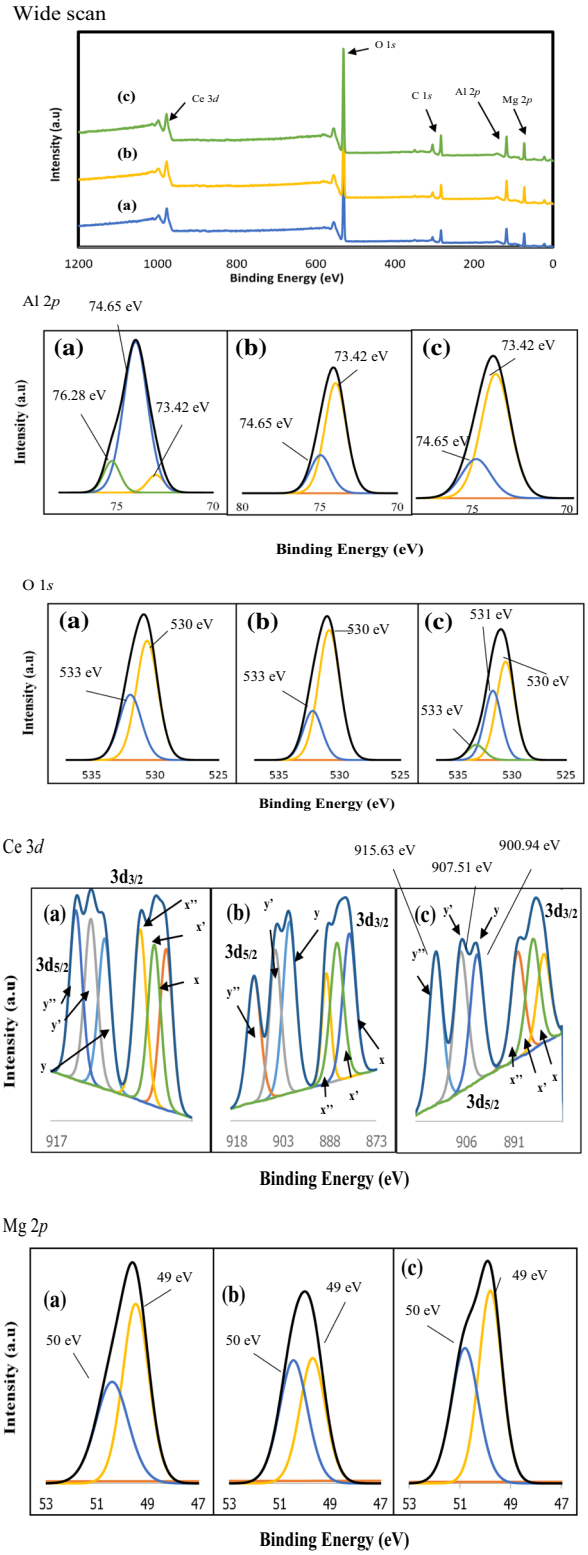

Fig. 6 The wide scan, Al 2*p*, O 1 *s*, Ce 3*d* and Mg 2*p* of XPS spectra for **a** Ru/Mg/Ce (10:30:60)/Al_2O_3 (500 °C), **b** Ru/Mg/Ce (10:30:60)/Al_2O_3 (600 °C) and **c** Ru/Mg/Ce (10:35:55)/Al_2O_3 (600 °C)

these findings are in good agreement with the XRD results displayed in Fig. 5, which revealed the species of Al_2O_3, CeO_2, and $Mg(Al_2O_4)$ from the prepared catalyst. This was attributed to $Mg(Al_2O_4)$ species that possessed greater mass concentration (0.76%) than MgO species (0.54%). Therefore, only $Mg(Al_2O_4)$ was observed in the XRD analysis.

3.3.4 FESEM-EDX Analysis

Generally, all the prepared catalysts showed rough surface morphology with irregular size and undefined shape. The images in Fig. 7a and b were resulted using different ratios. Figure 7a shows that the particles were not adequately dispersed and appeared densely packed on the catalyst surface, when compared to those in Fig. 7b. When Ce loading was increased by 5 wt.% (see Fig. 7b), the morphology of the catalyst was altered to aggregation and agglomeration. This morphology increased the catalytic activity of Ru/Mg/Ce (10:35:55)/Al_2O_3 catalyst (67.11%) to 79.04% over Ru/Mg/Ce (10:30:60)/Al_2O_3 catalyst. The uneven surface contributed to the high catalytic activity due to its easy access for the adsorbed molecules to react on the surface [36–38].

The result corroborated with XRD analysis, which showed that the crystallinity increased the agglomeration of Ru/Mg/Ce (10:30:60)/Al_2O_3 catalyst calcined at 600 °C (see Fig. 5). As a result of the effect of calcination temperature, the catalyst calcined at 500 °C (see Fig. 7c) showed a slightly different morphology when compared to the catalyst calcined at 600 °C (see Fig. 7b). The surface of the catalyst was unevenly distributed, with smaller particles dispersed between it and certain agglomerated particles. The smaller particles supported the XRD diffractograms, where Ru/Mg/Ce (10:30:60)/Al_2O_3 catalyst calcined at 500 °C was highly amorphous.

Table 6 displays the composition of elements for Ru/Mg/Ce/Al_2O_3 catalysts at different ratios and calcination temperatures. The elemental analysis showed the presence of Al, O, Ce, Mg, and Ru elements based on their respective weight ratio. Since alumina was used as support in this study, the weight percentage of Al was the second highest after O. From the EDX analysis, the composition of Mg was lower than Ru even though the catalyst was prepared with high composition of Mg rather than Ru. This phenomenon could be due to the smaller atomic size of alkaline earth metal Mg when compared to the atomic size of noble metal Ru. Therefore, it was presumed that the bigger atomic size of Ru covered the smaller atomic size of Mg on the surface, hence lowering the detection via EDX analysis.

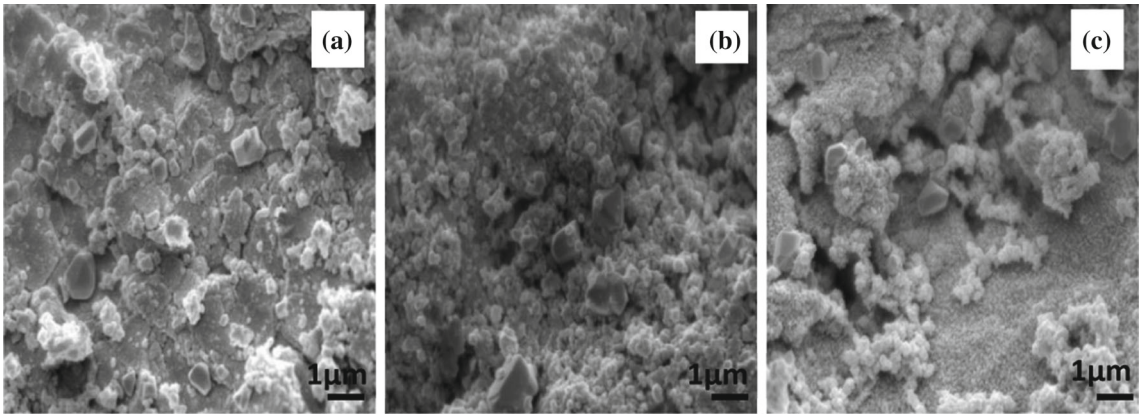

Fig. 7 FESEM micrographs of fresh **a** Ru/Mg/Ce (10:35:55)/Al_2O_3 (600 °C), **b** Ru/Mg/Ce (10:30:60)/Al_2O_3 (600 °C), **c** Ru/Mg/Ce (10:30:60)/Al_2O_3 (500 °C) catalysts with magnification; 10000X and scale bar; 1 µm

4 Conclusion

In this study, the promising catalyst was Ru/Mg/Ce/Al_2O_3 catalyst with ideal catalytic preparation conditions of 60 wt% of Ce loading at 600 °C calcination temperature for catalytic methanation reaction. This catalyst had converted 79.04% of CO_2 while forming 58.08% of CH_4. The experimental results were validated using CCD, which revealed that the best condition was 61 wt% of Ce loading at calcination temperature of 593 °C. The predicted value for CO_2 conversion given by this method was 78.82%, which was closer to the experimental results (79.04%). The characterisation technique using XRD revealed that Ru/Mg/Ce (10:30:60)/Al_2O_3 catalyst calcined at 600 °C was in an amorphous state with the presence of CeO_2, $Mg(Al_2O_4)$, and RuO_2 species as active species and this outcome was further supported through XPS analysis. Besides, the XPS analysis verified the presence of MgO species on the surface of the catalyst. The FESEM micrograph of Ru/Mg/Ce (10:30:60)/Al_2O_3 catalyst showed the aggregation and the agglomeration of smaller and larger particles that formed with a surface area of 147 m^2/g.

Acknowledgements The authors are gratefully acknowledged the Ministry of Higher Education for FRGS Vote 5F076 and Universiti Teknologi Malaysia for financial support under UTM-FR vote 21H03.

Author Contributions All authors contributed to the study conception and design. Siti Fadziana Sulaiman performed material preparation, data collection, and analysis. Wan Azelee Wan Abu Bakar supervised the research and checked the scientific contents of the manuscript. Wan Nur Aini Wan Mokhtar, Renugambaal Nadarajan, Khalida Muda, and Sarina Mat Rosid assisted in the characterisation of the catalysts and interpreted the data in RSM. Susilawati Toemen and Salmiah Jamal Mat Rosid wrote the first draft of the manuscript, and all authors commented on previous versions of the manuscript. All authors read and approved the final manuscript.

Declarations

Conflict of interest The authors report no declarations of interest.

References

1. Cao, X.: Climate change and energy development: implications for developing countries. Resour. Policy **29**(1), 61–67 (2003). https://doi.org/10.1016/j.resourpol.2004.05.001
2. Reddish, A.; Rand, M.: The environmental effects of present energy policies. In: Blunden, J.; Reddish, A. (Eds.) Energy resources and environment, pp. 43–91. Hodder and Stoughton & the Open University, London (1996)
3. Bahari, N.A.; Isahak, W.N.R.W.; Masdar, M.S.; Yaakob, Z.: Clean hydrogen generation and storage strategies via CO_2 utilization into chemicals and fuels: a review. Int. J. Energy Res. **43**(10), 5128–5150 (2019). https://doi.org/10.1002/er.4498
4. Ahmad, N.N.R.; Leo, C.P.; Mohammad, A.W.; Shaari, N.; Ang, W.L.: Recent progress in the development of ionic liquid-based mixed matrix membrane for CO_2 separation: a review. Int. J. Energy Res. **45**(7), 9800–9830 (2021). https://doi.org/10.1002/er.6518
5. Bukhari, S.N.; Chong, C.C.; Setiabudi, H.D.; Ainirazali, N.; Aziz, M.A.A.; Teh, L.P.; Annuar, N.H.R.: Comparative study of Ni loading methods towards superior CO_2 conversion over Ni/SBA-15. Int. J. Eng. Technol. **7**, 1663–1665 (2018). https://doi.org/10.14419/ijet.v7i4.38.29228
6. Rosid, S.J.M.; Toemen, S.; Abu Bakar, W.A.W.; Zamani, A.H.; Mokhtar, W.N.A.W.: Physicochemical characteristic of neodymium oxide-based catalyst for in-situ CO_2/H_2 methanation reaction. J. Saudi Chem. Soc. **23**(3), 284–293 (2019). https://doi.org/10.1016/j.jscs.2018.08.002
7. Muroyama, H.; Tsuda, Y.; Asakoshi, T.; Masitah, H.; Okanishi, T.; Matsui, T.; Eguchi, K.: Carbon dioxide methanation over Ni catalysts supported on various metal oxides. J. Catal. **343**, 178–184 (2016). https://doi.org/10.1016/j.jcat.2016.07.018

8. Zhou, G.; Liu, H.; Cui, K.; Jia, A.; Hu, G.; Jiao, Z.; Liu, Y.; Zhang, X.: Role of surface Ni and Ce species of Ni/CeO_2 catalyst in CO_2 methanation. Appl. Surf. Sci. **383**, 248–252 (2016). https://doi.org/10.1016/j.apsusc.2016.04.180
9. Konishcheva, M.V.; Potemkin, D.I.; Badmaev, S.D.; Snytnikov, P.V.; Paukshtis, E.A.; Sobyanin, V.A.; Parmon, V.N.: On the mechanism of CO and CO_2 methanation over Ni/CeO_2 catalysts. Top. Catal. **59**, 1424–1430 (2016). https://doi.org/10.1007/s11244-016-0650-7
10. Wu, J.C.S.; Chou, H.C.: Bimetallic Rh-Ni/BN catalyst for methane reforming with CO_2. Chem. Eng. J. **148**(2), 539–545 (2009). https://doi.org/10.1016/j.cej.2009.01.011
11. Toemen, S.; Bakar, W.A.W.A.; Ali, R.: Investigation of Ru/Mn/Ce/Al_2O_3 catalyst for carbon dioxide methanation: catalytic optimization, physicochemical studies and RSM. J. Taiwan Inst. Chem. Eng. **45**(5), 2370–2378 (2014). https://doi.org/10.1016/j.jtice.2014.07.009
12. Rao, G.R.; Mishra, B.G.: Structural redox and catalytic chemistry of ceria based materials. Bull. Catal. Soc. India **2**, 122–134 (2003)
13. Buang, N.A.; Abu Bakar, W.A.W.; Marsin, F.M.; Razali, M.H.: CO_2/H_2 methanation on nickel oxide based catalyst doped with various elements for the purification. Malays. J. Anal. Sci. **12**(1), 217–223 (2008)
14. Ocampo, F.; Louis, B.; Kiwi-Minsker, L.; Roger, A.-C.: Effect of Ce/Zr composition and noble metal promotion on nickel based $Ce_xZr_1-xO_2$ catalysts for carbon dioxide methanation. Appl. Catal. A Gen. **392**(1–2), 36–44 (2011). https://doi.org/10.1016/j.apcata.2010.10.025
15. Rosid, S.J.M.; Bakar, W.A.W.A.; Ali, R.: Characterization and modelling optimization on methanation activity using Box-Behnken design through cerium doped catalysts. J. Clean. Prod. **170**, 278–287 (2018). https://doi.org/10.1016/j.jclepro.2017.09.073
16. Zamani, A.H.; Shohaimi, N.A.M.; Rosid, S.J.M.; Abdullah, N.H.; Shukri, N.M.: Enhanced low temperature reaction for the CO_2 methanation over Ru promoted Cu/Mn on alumina support catalyst using double reactor system. J. Taiwan Inst. Chem. Eng. **96**, 400–408 (2019)
17. Myers, R.H.; Khuri, A.I.; Vining, G.: Response surface alternative to the Taguchi robust parameter design approach. Am. Stat. **46**(2), 131–139 (1992). https://doi.org/10.2307/2684183
18. Perego, C.; Villa, P.: Catalyst preparation methods. Catal. Today **34**(3–4), 281–305 (1997)
19. Yaccato, K.; Carhart, R.; Hagemeyer, A.; Lesik, A.; Strasser, P.; Volpe, A.F.; Turner, H.; Weinberg, H.; Grasselli, R.K.; Brooks, C.: Competitive CO and CO_2 methanation over supported noble metal catalysts in high throughout scanning mass spectrometer. Appl. Catal. A Gen. **296**, 30–48 (2005). https://doi.org/10.1016/j.apcata.2005.07.052
20. Kousha, M.; Tavakoli, S.; Danesha, E.: Central composite design optimization of acid blue 25 dye biosorption using shrimp shell biomass. J. Mol. Liq. **207**, 266–273 (2015). https://doi.org/10.1016/j.molliq.2015.03.046
21. Azhari, A.W.; Sopian, K.; Che Halin, D.S.; Ibrahim, A.H.; Zaidi, S.H.: Response surface methodology (RSM) in fabrication of nanostructured silicon. Mater. Sci. Forum. **857**, 151–155 (2016)
22. Yue, S.; Qiyan, F.; Xiangdong, L.: Application of response surface methodology to optimize degradation of polyacrylamide in aqueous solution using heterogeneous fenton process. Desalin. Water Treat. **53**(7), 1–10 (2013). https://doi.org/10.1080/19443994.2013.856351
23. Rosid, S.J.M.; Bakar, W.A.W.A.; Ali, R.: Methanation reaction over samarium oxide based catalysts. Mal. J. Fund. Appl. Sci. **9**(1), 28–34 (2013). https://doi.org/10.11113/mjfas.v9n1.78
24. Bakar, W.A.W.A.; Ali, R.; Toemen, S.: investigation of carbon dioxide methanation over ceria based catalysts. J. Teknol. **70**(1), 75–80 (2014). https://doi.org/10.11113/jt.v70.3418
25. Yang, S.; Wu, Y.M.: One step synthesis of methyl isobutyl ketone over palladium supported on $AlPO_4$-11 and SAPO-11. Appl. Catal. A Gen. **192**, 211–220 (2000). https://doi.org/10.1016/S0926-860X(99)00408-1
26. Oh, S.W.; Bang, H.Y.; Bae, Y.C.; Sun, Y.K.: Effect of calcinations temperature on morphology, crystallinity and electrochemical properties of nano-crystalline metal oxides (Co_3O_4, CuO and NiO) prepared via ultrasonic spray pyrolysis. J. Power Sources **173**, 502–509 (2007). https://doi.org/10.1016/j.jpowsour.2007.04.087
27. Zheng, H.Y.; An, M.Z.; Lu, J.F.: Surface characterization of the Zn-Al-Al_2O_3 nanocomposite coating fabricated under ultrasound condition. Appl. Surf. Sci. **254**, 1644–1650 (2008). https://doi.org/10.1016/j.apsusc.2007.07.110
28. Miyakoshi, A.; Ueno, A.; Ichikawa, M.: XPS and TPD characterization of manganese-substituted iron-potassium oxide catalysts which are selective for dehydrogenation of ethylbenzene into styrene. Appl. Catal. A Gen. **219**, 249–258 (2001). https://doi.org/10.1016/S0926-860X(01)00697-4
29. Toemen, S.; Bakar, W.A.W.A.; Ali, R.: Effect of ceria and strontia over Ru/Mn/Al2O3 catalyst: catalytic methanation, physicochemical and mechanistic studies. J. CO2 Util. **13**, 38–49 (2016)
30. Chang, F.-M.; Brahma, S.; Huang, J.-H.; Wu, Z.-Z.; Lo, K.-Y.: Strong correlation between optical properties and mechanism in deficiency of normalized self-assembly ZnO nanorods. Nature **9**, 905 (2019). https://doi.org/10.1038/s41598-018-37601-8
31. Kloprogge, J.T.; Wood, B.J.: X-ray photoelectron spectroscopic and Raman microscopic investigation of the variscite group minerals: variscite, strengite, scorodite and mansfieldite. Spectrochim. Acta Part A Mol. Biomol. Spectrosc. **185**, 163–172 (2017)
32. Wasalathanthri, N.D.; Poyraz, A.S.; Biswas, S.; Meng, Y.; Kuo, C.; Kriz, D.A.; Suib, S.L.: High-performance catalytic CH_4 oxidation at low temperatures : Inverse micelle synthesis of amorphous mesoporous manganese oxides and mild transformation to $K_{2-x}Mn_8O_{16}$ and ϵ-MnO_2. J. Phys. Chem. C **119**, 1473–1482 (2015)
33. Truffault, L.; Ta, M.T.; Devers, T.; Konstantinor, K.; Harel, V.; Simmonard, C.; Andreazza, C.; Neurkoveti, L.P.; Pinear, A.; Verun, D.: Application of nanostructured Ca doped CeO_2 for ultraviolet filtration. Mater. Res. Bull. **45**, 527–535 (2010). https://doi.org/10.1016/j.materresbull.2010.02.008
34. Shahed, S.M.F.; Hasegawa, T.; Sainoo, Y.: STM and XPS study of CeO_2(111) reduction by atomic hydrogen. Surf. Sci. **628**, 30–35 (2014). https://doi.org/10.1016/j.susc.2014.05.008
35. Kasten, L.S.; Grant, J.T.; Grebasch, N.; Voevodin, N.; Arnold, F.E.; Donley, M.S.: An XPS study of cerium dopants in sol-gel coatings for aluminium 2024–T3. Surf. Coat. Technol. **140**, 11–15 (2001). https://doi.org/10.1016/S0257-8972(01)01004-0
36. Ardizzone, S.; Bianchi, C.L.; Fadoni, M.; Vercelli, B.: Magnesium salts and oxide: an XPS overview. Appl. Surf. Sci. **119**, 253–259 (1997). https://doi.org/10.1016/S0169-4332(97)00180-3
37. Wan Abu Bakar, W.A.; Ali, R.; Toemen, S.: Catalytic methanation reaction over supported nickel-ruthenium oxide base for purification of simulated natural Gas. Sci. Iran **19**(3), 525–534 (2012). https://doi.org/10.1016/j.scient.2012.02.004
38. Wan Abu Bakar, W.A.; Ali, R.; Toemen, S.: Effect of Strontium on the Catalytic Activity and Physicochemical Properties of Ru/Mn Catalysts for CO_2 Methanation Reaction. Adv. Mater. Res. **1107**, 371–376 (2015)